CD244+ polymorphonuclear myeloid-derived suppressor cells reflect the status of peritoneal dissemination in a colon cancer mouse model

YUTAKA SUGITA[1], KIMIHIRO YAMASHITA[1], MITSUGU FUJITA[1,2], MASAFUMI SAITO[3], KOTA YAMADA[1], KYOSUKE AGAWA[1], AKIHIRO WATANABE[1], EIJI FUKUOKA[4], HIROSHI HASEGAWA[1], SHINGO KANAJI[1], TARO OSHIKIRI[1], TAKERU MATSUDA[1], TETSU NAKAMURA[1], SATOSHI SUZUKI[5] and YOSHIHIRO KAKEJI[1]

[1]Division of Gastrointestinal Surgery, Department of Surgery, Kobe University Graduate School of Medicine, Kobe, Hyogo 650-0017; [2]Center for Medical Education and Clinical Training, Kindai University Faculty of Medicine, Osakasayama, Osaka 589-8511; [3]Department of Disaster and Emergency and Critical Care Medicine, Kobe University Graduate School of Medicine, Kobe, Hyogo 650-0017; [4]Department of Gastroenterological Surgery, Hyogo Cancer Center, Akashi, Hyogo 673-8558; [5]Division of Community Medicine and Medical Network, Department of Social Community Medicine and Health Science, Kobe University Graduate School of Medicine, Kobe, Hyogo 650-0017, Japan

Received January 8, 2021; Accepted March 29, 2021

DOI: 10.3892/or.2021.8057

Abstract. Despite the recent development of chemotherapeutic agents, the prognosis of colorectal cancer (CRC) patients with peritoneal dissemination (PD) remains poor. The tumor immune microenvironment (TIME) has drawn attention as a key contributing factor of tumor progression. Of TIME components, myeloid-derived suppressor cells (MDSCs) are considered to play a responsible role in the immunosuppressive characteristics of the TIME. MDSCs are classified into two major subsets: Monocytic MDSCs (M-MDSCs) and polymorphonuclear MDSCs (PMN-MDSCs). Therefore, we hypothesize that MDSCs would play important roles in the PD-relevant TIME and PD progression. To address this hypothesis, we established PD mouse models. As the PD nodules consisted scarcely of immune cells, we focused on the peritoneal cavity, but not PD nodule, to evaluate the PD-relevant TIME. As a result, intraperitoneal PMN-MDSCs were found to be substantially increased in association with PD progression. Based on these results, we phenotypically and functionally verified the usefulness of CD244 for identifying PMN-MDSCs. In addition, the concentrations of interleukin (IL)-6 and granulocyte-colony stimulating factor (G-CSF) were significantly increased in the peritoneal cavity, both of which were produced by the tumors and thought to contribute to the increases in the PMN-MDSCs. *In vivo* depletion of the PMN-MDSCs by anti-Ly6G monoclonal antibody (mAb) significantly inhibited the PD progression and reverted $CD4^+$ and $CD8^+$ T cells in the peritoneal cavity and the peripheral blood. Collectively, these results suggest that the targeted therapy for PMN-MDSCs would provide not only new therapeutic value but also a novel strategy to synergize with T-cell-based immunotherapy for CRC-derived PD.

Introduction

Colorectal cancer (CRC) is the third most common cancer and the second most common cause of death worldwide (1). The prognosis of early-stage CRC is relatively favorable; 70-80% are eligible for curative-intent surgery, with a 5-year survival of 72-93% for stages I-II. In contrast, approximately 25% of CRC patients have metastases at the time of diagnosis; nearly 10% of those have synchronous peritoneal metastases (2,3). In addition, 8.3% of CRC patients have peritoneal dissemination (PD) regardless of synchronous or metachronous metastases (4). PD is a progressive and intractable state of CRC that is related to a poor prognosis. Despite the recent development of chemotherapeutic agents, the median survival of CRC patients with PD treated with systemic chemotherapy is 10-16 months after diagnosis, which is much shorter than the median survival of those with other organ metastases derived from CRC (5,6). Therefore, it is essential to elucidate

Correspondence to: Dr Kimihiro Yamashita, Division of Gastrointestinal Surgery, Department of Surgery, Kobe University Graduate School of Medicine, 7-5-2 Kusunoki-cho, Chuo-ku, Kobe, Hyogo 650-0017, Japan
E-mail: kiyama@med.kobe-u.ac.jp

Dr Mitsugu Fujita, Center for Medical Education and Clinical Training, Kindai University Faculty of Medicine, 377-2 Ohno-Higashi, Osakasayama, Osaka 589-8511, Japan
E-mail: mfujita47@gmail.com

Key words: myeloid-derived suppressor cell, polymorphonuclear myeloid-derived suppressor cell, neutrophil, CD244, peritoneal dissemination, colon cancer

the underlying mechanisms of the generation and progression of PD to identify effective therapeutic targets.

The tumor immune microenvironment (TIME) has drawn attention as a key contributing factor of tumor progression (7). The TIME consists of immune, vascular, and mesenchymal cells, as well as structural extracellular matrix proteins such as collagen, laminin, fibronectin, proteoglycans; it also contains soluble components such as metabolites, growth factors, cytokines, chemokines, and proteases (8-10). These components surround tumor cells, interact with each other, and work as a tumor-promoting ecosystem. Of note, TIME components in metastatic lesions differ from those in the primary lesions of the same cancer (8). Likewise, the TIME in PD is assumed to differ from that of primary or metastatic lesions. When PD occurs, tumor cells are isolated from the primary lesion, migrate in the peritoneal cavity, adhere to peritoneal mesothelial cells, and grow. Given the confined but spacious peritoneal cavity, ascitic flow primarily affects cell migration and the immune context of PD progression. From this viewpoint, ascites or peritoneal lavage is considered a feasible but important material to analyze the unique immune cell context of the PD-relevant TIME.

Of all TIME components, myeloid-derived suppressor cells (MDSCs) are considered to play a responsible role in the immunosuppressive characteristics of the TIME. MDSCs consist of immature myeloid cells in the early stages of differentiation to mature into macrophages, dendritic cells, and granulocytes (11). In the TIME, MDSCs immunologically promote tumor progression by suppressing the activation and function of T cells (12). In this regard, we previously reported that the accumulation of MDSCs in tumor sites, lung, and spleen correlates with tumor progression (13) and that the frequency of MDSCs in the peripheral blood correlates with tumor recurrence after surgical resection in mice (14). However, few studies have demonstrated whether and how MDSCs affect the generation and progression of PD.

MDSCs are classified into two major subsets: Monocytic MDSCs (M-MDSCs) and polymorphonuclear MDSCs (PMN-MDSCs) (15). The surface antigen phenotype of M-MDSCs is defined as $CD11b^{+}Ly6C^{high}Ly6G^{-}$ in mice, whereas that of PMN-MDSCs is $CD11b^{+}Ly6C^{low}Ly6G^{+}$ in mice, which is identical to that of normal neutrophils. Recently, CD244 has been highlighted as a surface antigen to distinguish PMN-MDSCs from normal neutrophils (11,16-18). Here, CD244 is an immunoregulatory transmembrane receptor molecule that belongs to the signaling lymphocyte activation molecule (SLAM) family (18). It is known to be expressed on natural killer (NK) cells and $CD8^{+}$ T cells (19,20). Recently, PMN-MDSCs isolated from tumor-bearing mouse have been shown to have substantially higher expression levels of CD244 than neutrophils isolated from naïve mouse. Also, sorted $CD244^{+}$ cells have shown higher immune-suppressive activities than $CD244^{-}$ cells (21). Thereafter, CD244 has been used as the most reliable marker to distinguish PMN-MDSCs from normal neutrophils (17).

These findings led us to hypothesize that $CD244^{+}$ MDSCs (PMN-MDSCs) may play a key role in the pathogenesis of PD and be an effective therapeutic target of PD. To this end, we established a PD mouse model and extensively analyzed cytokines as well as immune cells in the peritoneal lavage to evaluate the PD-relevant TIME. We also conducted PMN-MDSC elimination *in vivo* to confirm the therapeutic impacts on PD.

Materials and methods

Cell lines. The C57BL/6J mouse-derived colon cancer cell line MC38 was originally established by Dr F. James Primus at Beckman Research Institute, Duarte, CA, USA (22); Dr Toshiyasu Ojima at Wakayama Medical University, Wakayama, Japan kindly provided us this cell line (23). Luciferase-tagged line MC38 (MC38-luc) was generated as follows. MC38 cells were transfected with a CMV-GFP-T2A-luciferase pre-packaged lentivirus vector system BLIV101VA (System Biosciences, LLC). The cell lines stably expressing high levels of GFP and luciferase were established by sorting cells after the lentiviral infections. The BALB/c mouse-derived colon cancer cell line CT26 was obtained from American Type Culture Collection (ATCC). The MC38, MC38-luc, and CT26 cells were maintained in RPMI-1640 medium supplemented with 10% (v/v) heat-inactivated fetal bovine serum (FBS) (Sigma-Aldrich; Merck KGaA) at 37˚C in 5% CO_2. Cultured cells were confirmed negative for mycoplasma and viral contamination.

Mice. All animal experiments in this study were conducted with the approval of the Institutional Animal Care and Use Committee of Kobe University (approval no. P190404) in accordance with the ARRIVE guideline (24). Female C57BL/6J wild-type and BALB/c wild-type mice were purchased from CLEA Japan. OT-1 C57BL/6 transgenic mice were purchased from Charles River. All mice were maintained in pathogen-free conditions, fed *ad libitum*, and had free access to water in quiet humidified rooms on a 12:12-h light: Dark cycle. The mice were kept in plastic cages of 25x15x17 cm with five animals per cage. The health and behavior of mice were monitored once a day. Mice were acclimatized for at least five days before experiments. The administration of aspirin was used for analgesia, and inhalation using 4% isoflurane was used for anesthesia.

In vivo tumor models. *In vivo* experimental models of PD and subcutaneous inoculation (SC) were established by inoculating the corresponding strains of mice with the MC38, MC38-luc or CT26 cell lines. For survival analysis, female C57BL/6J mice were intraperitoneally or subcutaneously inoculated with $2x10^6$ MC38 cells and female BALB/c mice were intraperitoneally inoculated with $2x10^6$ CT26 cells. For sample collections of PD nodules, peritoneal lavage, spleens, and peripheral blood, $5x10^5$ MC38 cells or $1x10^5$ CT26 cells were transplanted as indicated above, and the tumor-bearing mice were sacrificed on Days 6, 13, and 20 after cell inoculation. Peritoneal lavage was conducted with 1.5 ml phosphate-buffered saline (PBS); spleens and peripheral blood were simultaneously collected. For an *ex vivo* antigen-specific T-cell suppression assay, spleens were harvested from OT-1 C57BL/6 transgenic mice and splenocytes were purified to use. For tumor volume analyses following Ly6G-mediated immune cell depletion, female C57BL/6 mice were intraperitoneally inoculated with $2x10^6$ MC38-luc cells and Ly6G mAb (clone 1A8; BioXCell) was

intraperitoneally injected at 200 μg/mouse every 3 days from Day 7 after the tumor inoculation. Control mice were treated with PBS with the same regimen.

From a viewpoint of animal welfare, the humane endpoints were set as follows: Difficulty in feeding and fluid intake, agonizing symptoms (self-injurious behavior, abnormal posture, breathing problems, crying), and marked abdominal distention. In addition, for the subcutaneous inoculation (SC) model, the following conditions were also considered: Tumor diameter >20 mm, tumor necrosis, ulceration, or tumor infection. Mice judged to have reached the humane endpoint were euthanized by cervical dislocation under anesthesia. Euthanasia was confirmed by their unresponsiveness to pain stimuli, apnea, and cardiac arrest. In this study, we used 74 C57BL/6J mice and 46 BALB/c mice in total. Most of the mice were euthanized for analyses; 12 C57BL/6J mice and 7 BALB/c mice were found dead of tumor development.

Histological analyses. The procedure used in this study has been published previously (25). Briefly, PD nodules were harvested from the MC38-based PD model and placed in 10% formalin overnight. The tissues were dehydrated, embedded in paraffin, and sliced into 5-μm-thick sections. The sections were soaked in xylene, ethanol in a gradient concentration and then stained with hematoxylin and eosin solutions. After drying, the sections were observed and photographed by a florescence microscope IX71 (Olympus) at x40 and x200 magnification for the morphology of tumor cells and immune cells in the PD nodules.

Gross tumor burden evaluation. To evaluate the tumor burden of the PD models, the number of PD nodules was measured grossly and scored as follows: P0 for no nodules, P1 for 1-3 nodules, P2 for 4-9 nodules, and P3 for 10 or more nodules. To evaluate the tumor burden of the SC models, the maximum and minimum diameters of tumor masses were measured and the tumor volume (V) was calculated as follows: V=maximum diameter x (minimum diameter)^2/2.

In vivo lumino-imaging for tumor growth evaluation. Tumor growth of the MC38-luc derived tumors *in vivo* was quantitively evaluated by total flux of luminescence (photons/sec) every 2-3 days. Briefly, D-luciferin substrate (OZ Biosciences) was intraperitoneally injected into the mice at 10 min before the measurement of luciferase flux. Bioluminescent images were captured by an *In Vivo* Imaging System (IVIS; Xenogen) and normalized by Living Image software (Xenogen) with minimum and maximum radiances of 5x10^6 and 1x10^8 photons/sec, respectively.

Immune cell isolation. To isolate splenocytes, spleens were harvested, ground, and filtered with cell strainers consisting of a nylon mesh with 70-μm pores (BD Biosciences). To isolate intraperitoneal immune cells, the peritoneal cavity was washed with 1.5 ml PBS and the lavage fluid was filtered with cell strainers consisting of a nylon mesh with 100-μm pores. Red blood cells were lysed with lysis buffer (Sigma-Aldrich; Merck KGaA). PD nodules were minced into small pieces and digested in a 1 mg/ml collagenase D (Worthington) and 60 U/ml DNase I (Roche) solution at 37˚C for 30 min. The cell suspension was passed through cell strainers consisting of a nylon mesh with 40-μm pores and centrifuged at 500 x g for 5 min. After discarding the supernatant, the cells were resuspended with 5 ml of 40% Percoll (GE Healthcare), centrifuged at 500 x g for 10 min, and lysed with lysis buffer to obtain single cell suspensions. The cells were then stained with the antibodies described below.

Flow cytometry. The procedure used in this study has been published previously (14,26). Briefly, the following anti-mouse monoclonal antibodies were purchased from BD Biosciences: Ly6G-peridinin chlorophyll protein (PerCP)-Cy5.5 (1A8; 560602), Ly6C-fluorescein isothiocyanate (FITC) (AL-21; 553104), CD4-allophycocyanin (APC) (RM4-5; 553051), CD25-FITC (7D4; 553071), and CD19-APC (1D3; 550992). The following antibodies were purchased from BioLegend: CD45-FITC (30F-11;103108), CD45-PerCP-Cy5.5 (30F-11;103132),CD45-brilliantviolet(BV510)(30F-11;103138), CD11b-APC/Fire750 (M1/70;101262), CD244-Alexa Fluor 647 (2B4;133509), F4/80-phycoerythrin (PE) (BM8;123110), PD-L1-BV421 (10F.9G2;124315), CD8a-APC/Fire 750 (53-6.7;100766), CD8a-PE (53-6.7; 100708), CD127-BV510 (A7R34;135033), CD1d-PE (1B1;123509), and CD5-BV421 (53-7.3;100618). The isolated immune cells were stained in a 96-round-bottom-well plate for 20 min at 4˚C and washed with PBS containing 1% bovine serum albumin. Sorting of Ly6G$^+$CD244$^+$ and Ly6G$^+$CD244$^-$ cells was conducted on a FACSAria instrument (BD Biosciences). Flow cytometric data were obtained by a FACS Verse instrument (BD Biosciences) and analyzed by FlowJo software (TreeStar, Inc.). CD45-gated cells were analyzed in this study.

Analysis of gene expression by quantitative real-time PCR. The procedure used in this study has been published previously (27-29); gene expression levels of Ly6G$^+$CD244$^+$ and Ly6G$^+$CD244$^-$ cells were assessed by quantitative real-time (q) PCR with the 2ΔCT method for relative quantitation of target genes to an internal control. Total RNA was extracted from the cells with TRIzol reagent (Invitrogen) and reverse transcribed into complementary DNA (cDNA) using a High-Capacity cDNA Reverse Transcription kit (Applied Biosciences). qPCR was conducted on a Takara Thermal Cycler Dice Real-time System (Takara Bio Inc.) with specific primers (Table I) and KOD SYBR qPCR Mix (Toyobo) according to the manufacturer's instructions. The thermal cycling conditions consisted of 95˚C for 30 sec, 40 cycles of 95˚C for 5 sec, and 60˚C for 30 sec. Amplification of glyceraldehyde 3-phosphate dehydrogenase (GAPDH) was used as the internal control.

Antigen-specific T cell suppression assay. The procedure used in this study has been published previously (21). Briefly, splenocytes of OT-1 C57BL/6 transgenic mice were purified, labeled with 125 nM carboxyfluorescein diacetate succinimidyl ester (CFSE; Invitrogen; Thermo Fisher Scientific, Inc.), seeded at 5x10^5 cells/well in 48-well plates, and co-cultured with Ly6G$^+$CD244$^+$ or Ly6G$^+$CD244$^-$ cells at indicated ratios in a complete medium [RPMI-1640 medium with 10% (v/v) heat-inactivated FBS, 1% penicillin/streptomycin, and 50 μM 2-mercaptoethanol] with 1 μg ovalbumin (OVA)-derived peptide SIINFEKL at 37˚C in 5% CO_2 for 48 h. The CFSE

Table I. Gene-specific primers used in qPCR.

Gene	Forward primer	Reverse primer
ARG1	CATGGGCAACCTGTGTCCTT	TCCTGGTACATCTGGGAACTTTC
NOS2	GACGAGACGGATAGGCAGAG	GTGGGGTTGTTGCTGAACTT
IL6	CCGGAGAGGAGACTTCACAG	TCCACGATTTCCCAGAGAAC
IL10	AAGGCAGTGGAGCAGGTGAA	CCAGCAGACTCAATACACAC
TGFB	CACCGGAGAGCCCTGGATA	TGTACAGCTGCCGCACACA
MPO	CCATGGTCCAGATCATCACA	GCCGGTACTGATTGTTCAGG
GAPDH	TGTGTCCCTCGTGGATCTGA	TTGCTGTTGAAGTCGCAGGAG

fluorescence of OT-1 $CD8^+$ T cells was measured by flow cytometry. All experiments were performed in triplicate.

Cytometric bead array assay. The procedure used in this study has been published previously (14). Briefly, we purchased cytometric bead array (CBA) assay kits from BD Biosciences. The plasma and supernatants of peritoneal lavage samples were collected, aliquoted into polypropylene microcentrifuge tubes, and stored at -80˚C until use. According to the manufacturer's protocol, the samples were mixed with antibody-coated capture beads against the following cytokines: Granulocyte colony-stimulating factor (G-CSF), granulocyte-macrophage colony-stimulating factor (GM-CSF), tumor necrosis factor-α (TNF-α), interferon (IFN)-γ, interleukin (IL)-1β, IL-2, IL-4, IL-6, IL-10, and IL-13. The samples were incubated for 1 h at room temperature, mixed with PE detection reagent, and further incubated for 1 h at room temperature. Then, the sample were washed, centrifuged at 500 x g for 5 min, and resuspended in assay buffer. The cytokine concentrations were measured by the FACSVerse instrument and FCAP Array software (BD Biosciences). All experiments were performed in duplicate and quantitated using a standardized curve.

Statistical analysis. Differences between two groups were analyzed using the Student's t-test. One-way analysis of variance (ANOVA) with Holm's *post-hoc* test was performed to analyze differences among multiple groups. Continuous variables are expressed as means. Survival curves were drawn using the Kaplan-Meier method and analyzed using the log-rank test. Statistical analyses were conducted using JMP software (version 10; SAS Institute). Values of $P<0.05$ were considered significant.

Results

Peritoneal dissemination is associated with poor prognosis of tumor-bearing hosts. We first established PD mouse models using the murine colon cancer cell lines MC38 (Fig. 1A) and CT26 (Fig. 1B). PD nodules became enlarged and increased in both models over time, with a slight predominance in the CT26-based model compared with the MC38 model (Table SI). Histopathological analyses of the MC38-based model revealed that the PD nodules consisted mostly of tumor cells and scarcely of immune cells (Fig. 1C). Consistent with the tumor burden evaluation (Table SI), survival analyses revealed that the prognosis of the CT26-based PD model was poorer than that of the MC38 (P=0.12) (Fig. 1D, red solid line vs. black solid line). Based on these results, we decided to use the MC38 cell line primarily in this study because of its feasibility of experimental handling. We also tested the MC38-based SC model (Table SII) to compare with the PD model. The prognosis of the PD model was significantly poorer than that of the SC tumor model (P=0.015) (Fig. 1D, red solid line vs. red dotted line). These results suggest that peritoneal dissemination is associated with poor prognosis of tumor-bearing hosts.

Next, we sought to compare the total amount of tumor burdens of the PD and SC models. As mentioned above (Tables SI and SII), the total tumor volume in the SC model was grossly measurable, whereas the total tumor volume in the PD model was extremely difficult to measure grossly due to the multiple nature of the PD model (Fig. 1E). Therefore, to the same end, we used the bioluminescent MC38-luc cell line and an *in vivo* bioluminescence detection system (Fig. 1F). Consistent with the survival data (Fig. 1D), total tumor burden was significantly increased in the PD model compared with the SC model (P=0.048) (Fig. 1G). Taken together, these results suggest that peritoneal dissemination is associated with poor prognosis of tumor-bearing hosts.

Intraperitoneal PMN-MDSCs substantially increase with PD progression. Based on the finding that immune cell infiltration was very rare in the PD nodules (Fig. 1C), we hypothesized that the peritoneal cavity through the systemic circulation would be the main site of immune responses for PD. To address this hypothesis, we evaluated immune cell profiles in the peritoneal cavity and the systemic circulation in detail using flow cytometry (Fig. 2A). Representative flow cytometric figures of the MC38-based model are provided (Fig. 2B). In the peritoneal cavity of the MC38-based PD model, the numbers of M-MDSCs and PMN-MDSCs were significantly increased with tumor progression (M-MDSCs: P=0.027 and PMN-MDSCs: P=0.046 for Day 0 vs. Day 20) (Fig. 2C, left panel, solid black line and dotted black line). The numbers of intraperitoneal PMN-MDSCs rapidly increased on Day 13 after tumor inoculation (Fig. 2C, left panel, solid black line). We also analyzed the MDSC subsets in the spleen and peripheral blood in both the MC38-based PD and SC models over time (Fig. 2D). As in the peritoneal cavity, the number of PMN-MDSCs in the peripheral blood increased after Day 13 in the PD model (Fig. 2D, right panel, red solid line). In comparison, M-MDSCs consistently had a numerical advantage over PMN-MDSCs in the SC model (Fig. 2D, dotted lines).

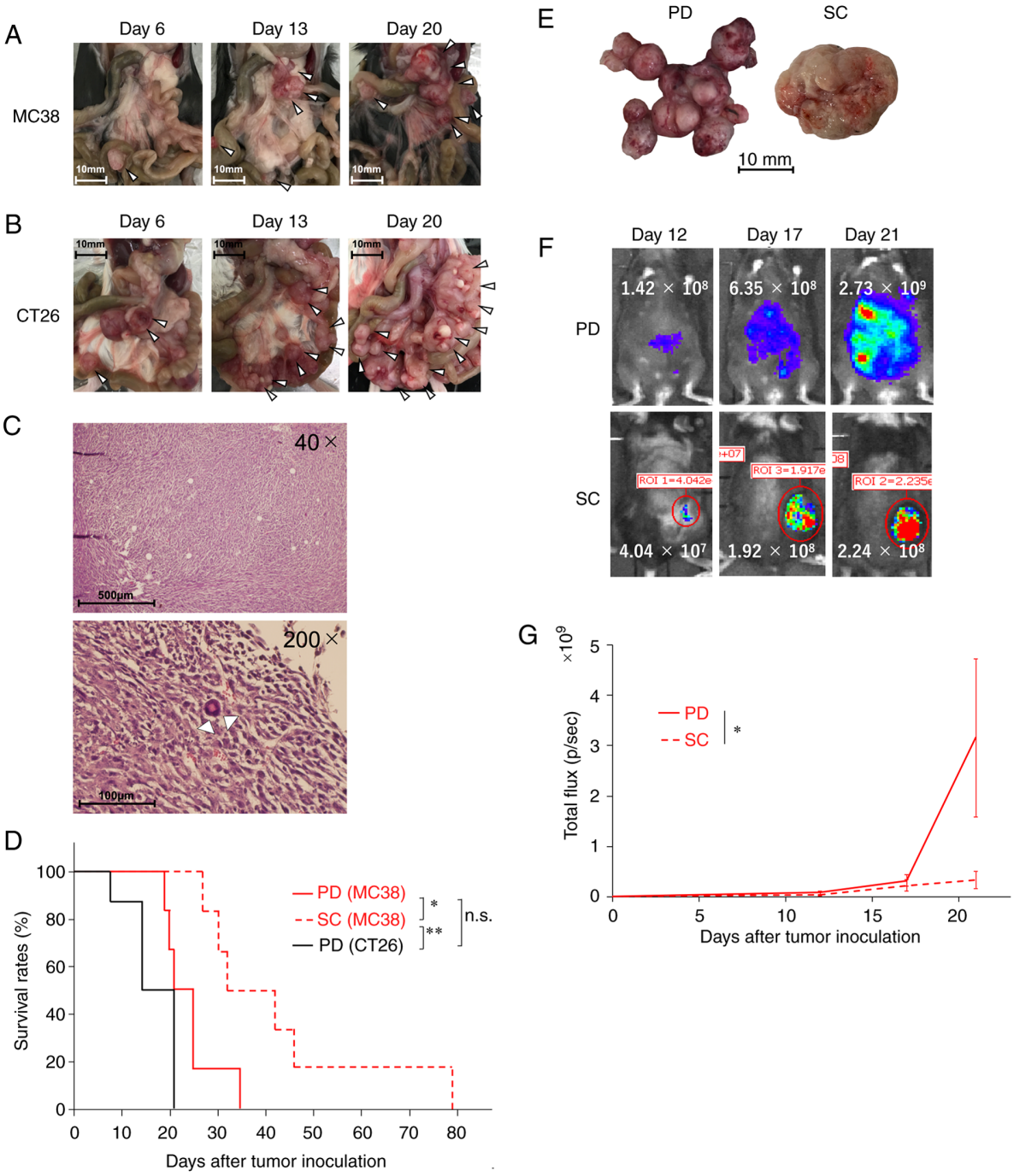

Figure 1. Peritoneal dissemination is associated with poor prognosis of tumor-bearing hosts. Female C57BL/6J or BALB/c mice (n=6) were intraperitoneally inoculated with $2x10^6$ MC38 or $1x10^5$ CT26 colon cancer cell line, respectively. The progression of peritoneal dissemination (PD) was evaluated over time. (A) Representative images of the MC38-based PD model on Days 6, 13 and 20. (B) Representative images of the CT26-based PD model on Days 6, 13 and 20. Arrowheads indicate PD nodules. (C) Histopathology of PD nodules of the MC38-based PD model. Magnification: x40 (upper) and x200 (lower). Arrowheads indicate the infiltrating immature polymorphonuclear cells. Female C57BL/6J mice (n=6) were subcutaneously (SC) inoculated with $2x10^6$ MC38 colon cancer cells, and (D) survival analysis of MC38-based PD and SC models, and CT-26 based PD models is shown. Log-rank test followed by Bonferroni correction was performed. (E) Representative images of tumor burdens obtained from the MC38-based PD model (left) and MC38-based SC model (right). Female C57BL/6J mice (n=6) were intraperitoneally or SC inoculated with $2x10^6$ MC38-luc cancer cells. (F) Representative luciferase bioluminescence images of the PD and the SC models on Days 12, 17 and 21. Numerical values in each image indicate the total flux of bioluminescence. (G) Time-course enumeration of the total flux (p/sec=photons/second) of the PD and the SC models. Values are expressed as mean values with standard errors. Two-way repeated measures ANOVA followed by Bonferroni correction was performed. $^*P<0.05$, $^{**}P<0.01$; n.s., not significant.

To confirm the results above, we complementarily tested the CT26-based PD models (Fig. 2E and F). Consistent with the MC38 data (Fig. 2D), longitudinal evaluations of flow cytometry demonstrated a rapid increase in the $Ly6G^+CD11b^+$ cell population, which has been shown to include $CD244^+$ PMN-MDSCs (21), in both the peritoneal cavity and the peripheral blood (Fig. 2F). Taken together, these results suggest that the local and/or systemic predominance of PMN-MDSCs is involved in the poor prognosis of the PD-bearing hosts.

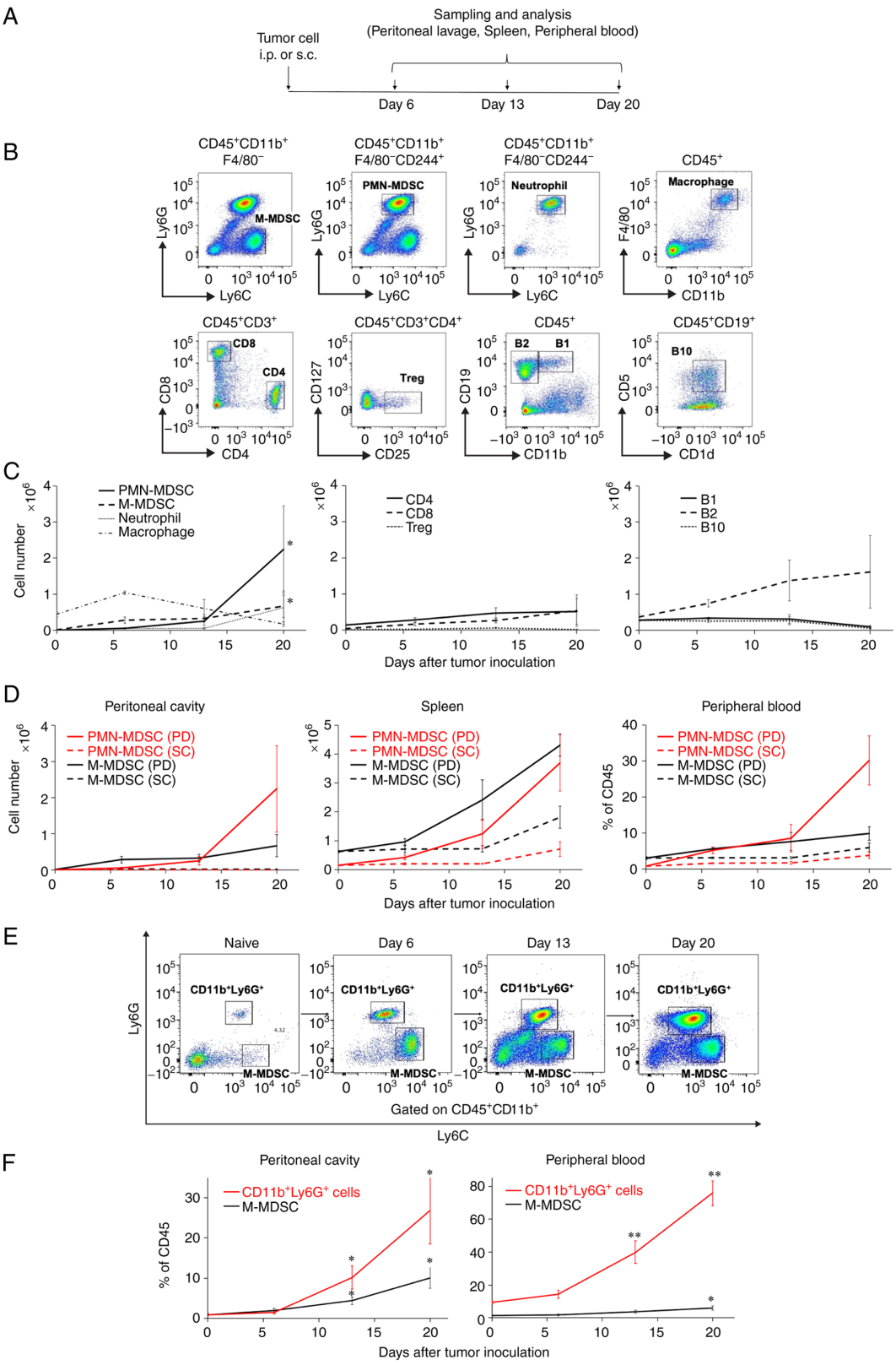

Figure 2. Intraperitoneal PMN-MDSCs substantially increase with PD progression. (A) Female C57BL/6J mice (n=6) were intraperitoneally (i.p.) or subcutaneously (s.c.) inoculated with $5x10^5$ MC38 colon cancer cells and sacrificed to collect peritoneal lavage, spleens, and peripheral blood on Days 6, 13 and 20 as indicated. (B) Representative flow cytometric data of intraperitoneal immune cell subsets. The cells were defined as follows: $CD11b^+F4/80^-Ly6C^{high}Ly6G^-$ for monocytic myeloid-derived suppressor cells (M-MDSCs), $CD11b^+F4/80^-CD244^+Ly6C^{mid}Ly6G^+$ for polymorphonuclear (PMN)-MDSCs, $CD11b^+F4/80^-CD244^-Ly6C^{mid}Ly6G^+$ for neutrophils, $CD11b^+F4/80^+$ for macrophages, $CD3^+CD4^+$ for CD4 T cells, $CD3^+CD8^+$ for CD8 T cells, $CD3^+CD4^+CD25^+CD127^-$ for regulatory T cells (Tregs), $CD19^+CD11b^+$ for B1 cells, $CD19^+CD11b^-$ for B2 cells, and $CD19^+CD1d^+CD5^+$ for B10 cells. (C) Time-course enumeration of the immune cell numbers identified. (D) Time-course enumeration of the number of MDSCs in the peritoneal cavity, spleen, and peripheral blood in the MC38-based peritoneal dissemination (PD) and subcutaneously (SC) inoculated models. Female BALB/c mice (n=4) were intraperitoneally inoculated with $1x10^5$ CT26 colon cancer cells and sacrificed to collect peritoneal lavage and peripheral blood on Days 6, 13 and 20. (E) Representative flow cytometric data of intraperitoneal $CD11b^+Ly6G^+$ cells and M-MDSCs. (F) Time-course enumeration of their frequencies in the peritoneal cavity and the peripheral blood. Values are expressed as mean values with standard errors. One-way ANOVA with Holm's *post-hoc* test was performed. $^*P<0.05$, $^{**}P<0.01$.

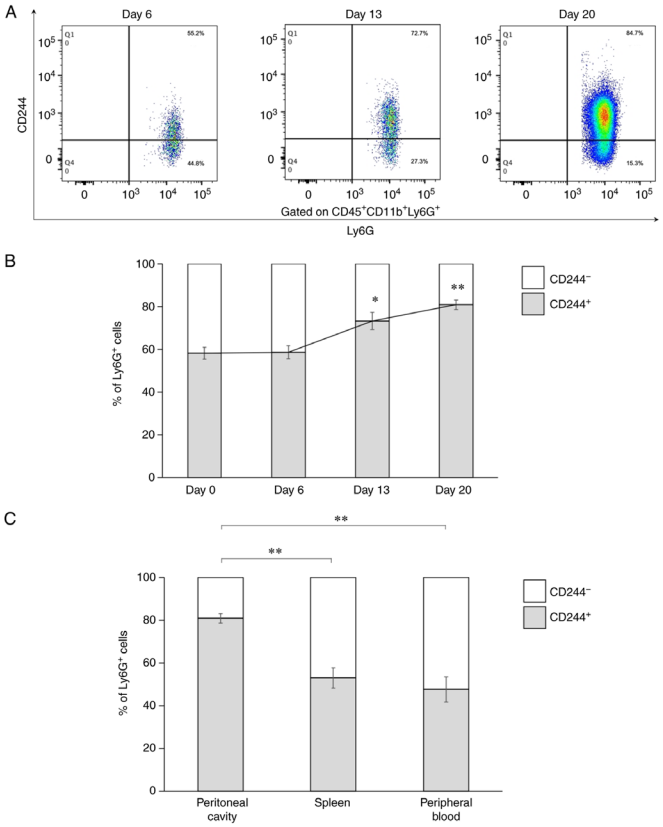

Figure 3. Intraperitoneal Ly6G$^+$CD11b$^+$ population predominantly consists of CD244$^+$ cells. The samples were collected from the MC38-based peritoneal dissemination (PD) model (n=6) as described in Fig. 2. The ratios of CD244$^+$ cells among CD11b$^+$F4/80$^-$Ly6C^{mid}Ly6G$^+$ cells were evaluated by flow cytometry. (A) Representative flow cytometric data of CD244$^+$ cells among the CD11b$^+$F4/80$^-$Ly6C^{mid}Ly6G$^+$ cells in the peritoneal cavity. (B) Time-course enumeration of the ratio of CD244$^+$ cells among Ly6G$^+$ cells. (C) Ratios of CD244$^+$ cells among Ly6G$^+$ cells in the peritoneal cavity, spleen, and peripheral blood on Day 20 after tumor inoculation. Values are expressed as mean values with standard errors. One-way ANOVA with Holm's *post-hoc* test was performed. *P<0.05, **P<0.01.

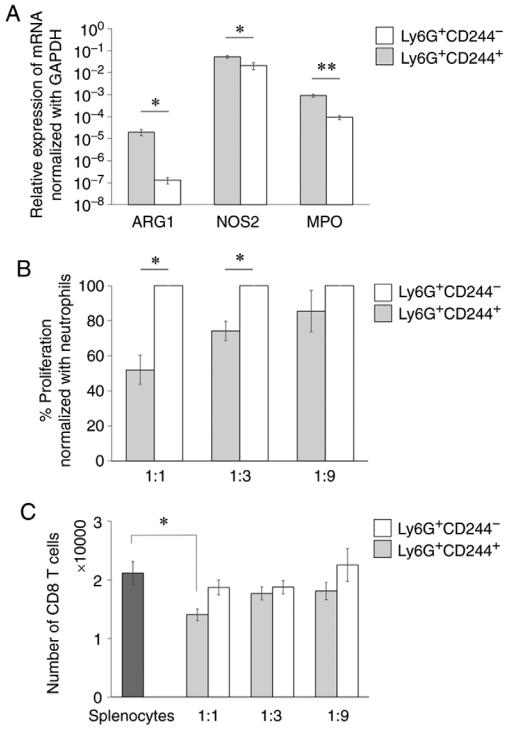

Figure 4. Ly6G$^+$CD244$^+$ cells function as PMN-MDSCs. Spleens were harvested from the MC38-based subcutaneous inoculation (SC) model at 20-30 days after tumor inoculation. Splenocytes were then purified. Ly6G$^+$CD244$^+$ and Ly6G$^+$CD244$^-$ cells were further isolated from the splenocytes by a FACS Aria instrument. (A) The gene expression levels of Arginase-1 (*ARG1*), nitric oxide synthase 2 (*NOS2*), and myeloperoxidase (*MPO*) in Ly6G$^+$CD244$^+$ and Ly6G$^+$CD244$^-$ cells were measured by quantitative real-time (q)PCR. GAPDH was used to normalize gene expression data. CFSE-labeled OT-1 splenocytes (5x10^5) were co-cultured with Ly6G$^+$CD244$^+$ or Ly6G$^+$CD244$^-$ cells at indicated ratios with SIINFEKL peptides. CFSE fluorescence of OT-1 CD8$^+$ T cells was measured by flow cytometry. (B) Proliferation rates of OT-1 CD8$^+$ T cells, normalized with Ly6G$^+$CD244$^-$ cells. (C) The total number of OT-1 CD8$^+$ T cells. Values are expressed as mean values with standard errors. Student's t-test was performed for two group comparisons. *P<0.05, **P<0.01. PMN-MDSCs, polymorphonuclear myeloid-derived suppressor cells.

Intraperitoneal Ly6G$^+$CD11b$^+$ population predominantly consists of CD244$^+$ cells. To confirm how the Ly6G$^+$CD11b$^+$ myeloid cell population consisted of CD244$^+$ PMN-MDSCs in this study (21), we evaluated the ratios of CD244$^+$ PMN-MDSCs in Ly6G$^+$ cells (Fig. 3). Representative flow cytometric figures of the MC38-based model are provided (Fig. 3A). The intraperitoneal Ly6G$^+$CD244$^+$ cells gradually increased over time (Fig. 3B), and the frequencies of the CD244$^+$ cells in the Ly6G$^+$ cells were significantly high on Days 13 and 20 in the tumor-bearing mice compared with Day 0 (P=0.011 on Day 13, P=0.0002 on Day 20). Also, the frequencies of the CD244$^+$ cells in the Ly6G$^+$ cells increased over time in the spleen and the peripheral blood (data not shown). Among the samples tested on Day 20, the peritoneal cavity showed the highest frequency of the CD244$^+$ cells in the Ly6G$^+$ cells (P=0.0007 vs. spleen, P=0.0007 vs. peripheral blood) (Fig. 3C). These results suggest that intraperitoneal CD244$^+$ PMN-MDSCs contributed to tumor progression and poor prognosis in the PD model.

Ly6G$^+$CD244$^+$ cells function as PMN-MDSCs. As the findings thus far suggest the functional importance of Ly6G$^+$CD244$^+$ cells, we subsequently addressed the immunological function of Ly6G$^+$CD244$^+$ cells to determine whether they function as PMN-MDSCs. To this end, we conducted qPCR to analyze the mRNA levels of the immunosuppressive genes in the Ly6G$^+$CD244$^+$ cells (Table I). The following immunosuppressive genes were significantly increased in the Ly6G$^+$CD244$^+$ cells: Arginase-1 (*ARG1*: P=0.030), nitric oxide synthase 2 (*NOS2*: P=0.036), and myeloperoxidase (*MPO*: P=0.005) (Fig. 4A). To confirm the immunosuppressive function of the Ly6G$^+$CD244$^+$ cells, we performed an *ex vivo* antigen-specific T-cell suppression assay. The Ly6G$^+$CD244$^+$ cells significantly inhibited antigen-specific CD8$^+$ T-cell proliferation compared with the Ly6G$^+$CD244$^-$ cells at high (1:1) and moderate (1:3) ratios (1:1: P=0.030, 1:3: P=0.017) (Fig. 4B). T-cell suppression meditated by the Ly6G$^+$CD244$^+$ cells was also observed in the numerical evaluation of CD8$^+$ T cells at a high (1:1) ratio (P=0.031) (Fig. 4C). These findings suggest that the Ly6G$^+$CD244$^+$ cells effectively suppressed T cells *ex vivo* and thus could be functionally considered as PMN-MDSCs.

PD nodules consist mostly of tumor cells and scarcely of immune cells. Histopathological analyses showed that immune

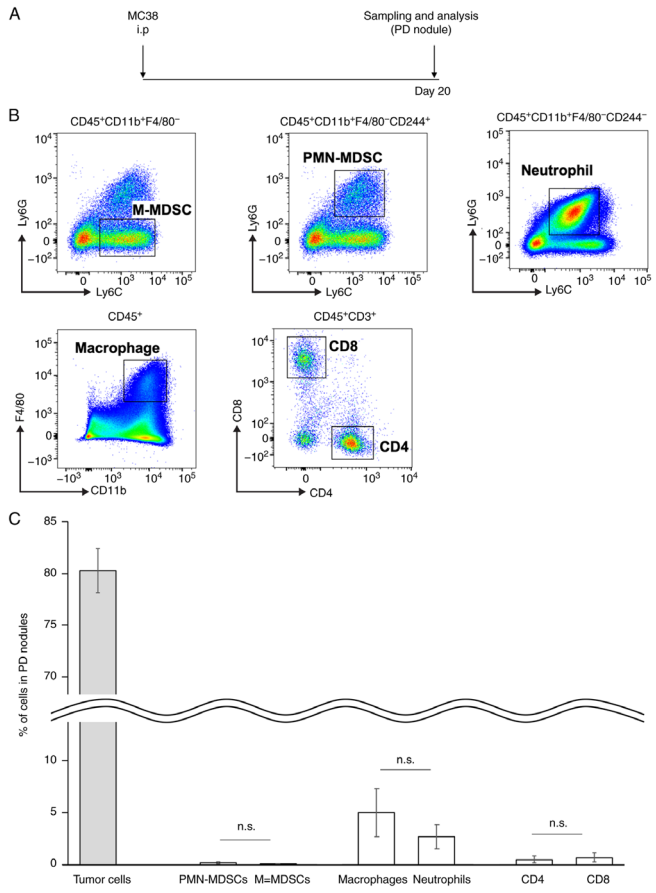

Figure 5. PD nodules consist mostly of tumor cells and scarcely of immune cells. (A) The MC38-based peritoneal dissemination (PD) model (n=3) was induced as described in Fig. 2, and the PD nodules were collected on Day 20 after tumor inoculation. (B) Representative flow cytometric data of the indicated immune cells. (C) The percentage of tumor cells and each immune cell subset in the PD nodules. Values are expressed as mean values with standard errors. Student's t-test was performed for two group comparisons. n.s., not significant; PMN-MDSCs, polymorphonuclear myeloid-derived suppressor cells; M-MDSCs, monocytic myeloid-derived suppressor cells.

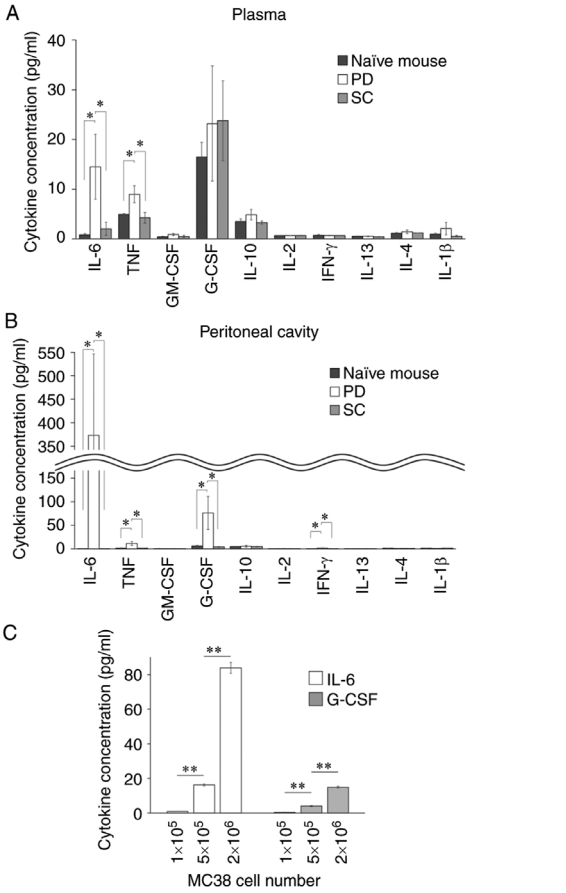

Figure 6. Tumor-derived cytokines are involved in the PMN-MDSC induction. The MC38-based peritoneal dissemination (PD) and subcutaneous inoculation (SC) models (n=6) were induced as described in Fig. 2, and the peritoneal lavage and peripheral blood were collected on Day 20 after tumor inoculation. Cytometric bead array (CBA) assays were conducted. (A) Cytokine concentrations in plasma. (B) Cytokine concentrations in the peritoneal cavity. (C) The concentrations of G-CSF and IL-6 in the culture supernatant of MC38 colon cancer cells at the indicated numbers were evaluated by the CBA assays. Values are expressed as mean values with standard errors. One-way ANOVA with Holm's *post-hoc* test was performed. $^{*}P<0.05$, $^{**}P<0.01$. PMN-MDSCs, polymorphonuclear myeloid-derived suppressor cells; IL, interleukin; TNF, tumor necrosis factor; G-CSF, granulocyte colony-stimulating factor; IFN-γ, interferon-γ.

cell infiltration was very rare in the PD nodules (Fig. 1C). To confirm this finding from a viewpoint of the CD244^{+} cells, we performed flow cytometric analyses of the PD nodules (Fig. 5A). Representative flow cytometric figures of the PD nodules in the MC38-based model are provided (Fig. 5B). Consistent with the histopathological findings (Fig. 1C), intratumoral PMN-MDSCs were detectable but accounted for only 0.1% of all cells (including tumor cells) in the PD nodules (Fig. 5C). Taken together, these findings support our hypothesis that the peritoneal cavity through the systemic circulation would be the main site of immune responses for PD.

Tumor-derived cytokines are involved in the PMN-MDSC induction. The finding above led us to investigate the causes of the increase in the intraperitoneal PMN-MDSCs. To this end, we conducted CBA assays using the ascites obtained on Day 20 to evaluate the levels of cytokines in the peritoneal cavity comprehensively (Fig. 6). The concentrations of IL-6 and TNF-α were significantly increased in the peritoneal cavity and plasma of the PD model (Fig. 6A and B). In addition, G-CSF was significantly increased in the peritoneal cavity (Fig. 6B). Similar to these *in vivo* data, MC38 tumor cells secreted IL-6 and G-CSF *in vitro*, and their production levels increased in a cell number-dependent manner (Fig. 6C). These results suggest that the presence of PD would induce unique immunological profiles, such as the increases in IL-6 and G-CSF, in the peritoneal cavity.

PMN-MDSC-targeting therapy reverts the number of T cells and suppresses the tumor progression in the PD model. To clarify the pathological functions of PMN-MDSCs in the PD model, we sought to deplete PMN-MDSCs in the PD model. In this regard, since PMN-MDSCs accounted for the large majority of Ly6G^{+} cells (Fig. 3) and *in vivo*-compatible anti-CD244 antibody is known to exert strong effects on natural killer (NK) and T cells inadvertently (30), we decided to use anti-Ly6G mAb to deplete PMN-MDSCs (Fig. 7A). As expected, *in vivo* administration of anti-Ly6G mAb completely depleted intraperitoneal Ly6G^{+} cells (Fig. 7B). Although the treatment with anti-Ly6G mAb did not prolong the survival of tumor-bearing mice (Fig. 7C), tumor progression was

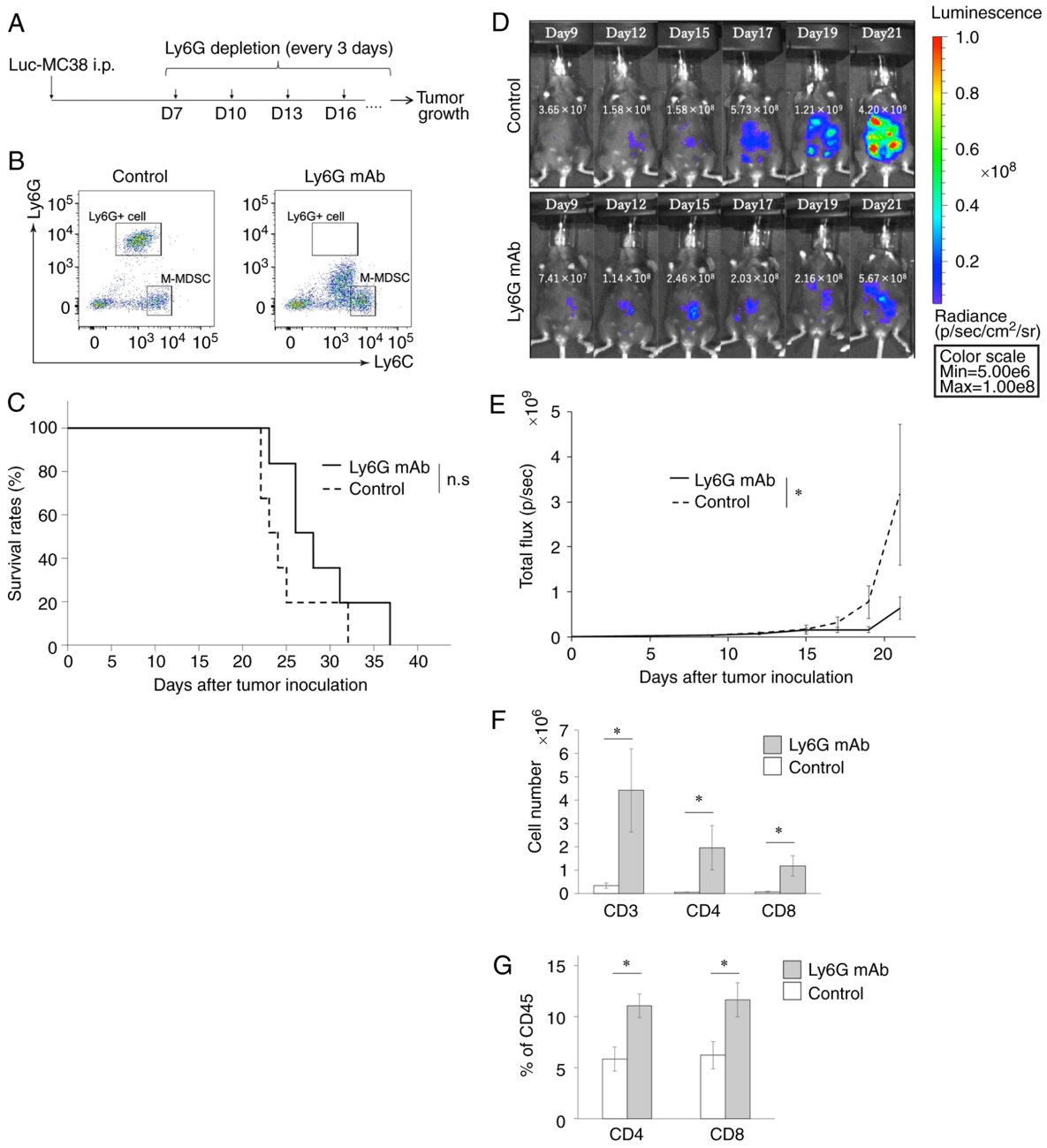

Figure 7. PMN-MDSC-targeting therapy reverts the number of T cells and suppresses the tumor progression in the peritoneal dissemination (PD) model. (A) Female C57BL/6J mice (n=6) were intraperitoneally (i.p.) inoculated with 2x10^6 MC38-luc cells. Anti-Ly6G mAb (clone 1A8) was intraperitoneally injected at 200 μg/mouse every 3 days from Day 7 after the tumor inoculation. Tumor growth was evaluated by an *In Vivo* Imaging System (IVIS) every 2-3 days. (B) Representative flow cytometric data of Ly6G$^+$ cells in the control and the treated groups on Day 17 after tumor inoculation. Ly6G$^+$ cells were effectively depleted in the treated group. (C) Survival analysis of the control and the treated groups. Log-rank test was performed. (D) Representative luciferase bioluminescence images of the control and the treated groups on Days 9, 12, 15, 17, 19 and 21. Numerical values in each image indicate the total flux of bioluminescence. (E) Time-course enumeration of the total flux (p/sec) of the control and the treated groups. Values are expressed as mean values with standard errors. Two-way repeated measures ANOVA followed by Bonferroni correction was performed. (F) The numbers of T cells in the peritoneal cavity on Day 19 after tumor inoculation. (G) The percentage of T cells in the peripheral blood on Day 19 after tumor inoculation. Student's t-test was performed for two group comparisons. *P<0.05; n.s., not significant; PMN-MDSCs, polymorphonuclear myeloid-derived suppressor cells; M-MDSC, monocytic myeloid-derived suppressor cell.

significantly suppressed in the mice treated with the anti-Ly6G mAb compared with control mice until Day 21 (P=0.025) (Fig. 7D and E). We also evaluated whether anti-Ly6G mAb would affect T-cell kinetics in the peritoneal cavity and the peripheral blood. The treatment with anti-Ly6G mAb significantly increased the number of both intraperitoneal CD3$^+$, CD4$^+$, and CD8$^+$ T cells of the tumor-bearing mice (CD3: P=0.037, CD4: P=0.037, CD8: P=0.025) (Fig. 7F). The peripheral blood showed the similar trends (CD4: P=0.025, CD8: P=0.037) (Fig. 7G). These results suggest that PMN-MDSCs suppress the antitumor activities of T cells to induce PD progression and that they may be a potent therapeutic target for PD.

Discussion

We clarified the pathological roles of peritoneal dissemination (PD)-associated polymorphonuclear myeloid-derived

suppressor cells (PMN-MDSCs) in this study. We previously demonstrated the associations of MDSCs with tumor progression (13,14), which led us to hypothesize that MDSCs may also play an important role in the PD-relevant tumor immune microenvironment (TIME). To address this hypothesis, we first established a PD mouse model. Based on the finding that the PD nodules consisted scarcely of immune cells, we focused on the peritoneal cavity, but not the PD nodule, to evaluate the PD-relevant TIME. Among the cell population evaluated, intraperitoneal PMN-MDSCs substantially increased in association with PD progression. The characteristics of PMN-MDSCs were phenotypically and functionally determined. In addition, the concentrations of interleukin (IL)-6 and granulocyte-colony stimulating factor (G-CSF) were significantly increased in the peritoneal cavity, which was produced by the tumors and thought to contribute to the increase in PMN-MDSCs. As PMN-MDSCs accounted for the large majority of $Ly6G^+$ cells, we conducted Ly6G-mediated PMN-MDSC depletion *in vivo*. The PMN-MDSC depletion significantly inhibited the progression of PD and reverted both $CD4^+$ and $CD8^+$ T cells in the peritoneal cavity and the peripheral blood. Taken together, these results suggest that targeted therapy for PMN-MDSCs would provide therapeutic values to prevent the disease progression of PD derived from colorectal cancer (CRC).

In this study, we tested two types of murine colon cancer cell lines (MC38 and CT26) to induce PD and observed similar results. The findings in this study are also consistent with those of previous studies that have analyzed the clinical samples derived from patients with gastric cancer (31), cervical cancer (32), and breast cancer (33). In addition, human cancers have extremely high heterogeneity, by which MDSCs can be induced through a wide variety of tumor-relevant mechanisms (34). Based on these findings, we believe that the findings in this study can be generalized at least to some extent. Particularly to address the heterogeneous conditions of PD, we are in the process of conducting an observational clinical study using the specimens of CRC-PD patients.

Regarding the comparison of total tumor volumes in the PD and subcutaneous inoculation (SC) models, we found it difficult to calculate the tumor volumes from photographic data in this study, particularly due to the multiple nature of the PD model. PD is characterized by tumor cells spreading widely in the abdominal cavity by the flow of ascites fluid (35). In fact, the number of PD nodules in the abdominal cavity reached more than 10 in a substantial number of the MC38-based PD models. In addition, the PD nodules of various sizes were observed, some of which were fused together. In order to compare the total tumor volumes in the SC and PD models under the same conditions, we measured the *in vivo* bioluminescence intensity using the bioluminescent MC38-luc cell line in both models. As a result, the PD models were found to have higher tumor volume and poorer prognosis than the SC models. Of note, it is well known that the *in vivo* bioluminescence intensity reflects the total number and quantity of luminescent materials including living cells in host animals (36). Such an *in vivo* bioluminescence detection system could be very useful for assessing the total tumor volume in multiple tumor models such as the PD model.

Immune cell infiltration in PD nodules was barely detectable in our animal model. Therefore, we concluded that detailed immunological evaluation of PD nodules was difficult to conduct. However, other investigators have reported that immune cells are detectable and reflect immune responses and treatment effects (37,38). The differences are that the number of tumor cells used in these studies was much smaller than in our fast-growing PD model. That is, rapidly growing tumors induce areas of hypoxia with low levels of glucose and nutrients, leading to lactic acid accumulation and eventually inhibiting the immune cells from infiltrating into the tumor tissue (39). In contrast, the lower the number of cells administered, the slower the disease progression and the more likely the immune response will occur. For this reason, the number of infiltrating immune cells may have been high in these studies. In this regard, further studies would be needed for an accurate immunological evaluation of PD nodules.

It has been a long-lasting question in the research field of MDSCs how to distinguish PMN-MDSCs from neutrophils in mice. Since CD244 has been highlighted as a surface antigen to identify PMN-MDSCs (11,16-18), we tested whether $Ly6G^+CD244^+$ cells would have immunosuppressive activity on T cells. As expected, $Ly6G^+CD244^+$ cells showed significantly higher gene expression levels of *ARG1*, *NOS2*, and *MPO* than $Ly6G^+CD\ 244^-$ cells. These genes are frequently evaluated as the immunosuppressive mediators representing PMN-MDSCs, along with positive correlations with the corresponding protein levels (27-29). Moreover, $Ly6G^+CD244^+$ cells suppressed T cells *ex vivo*. Based on these findings, we considered $Ly6G^+CD244^+$ cells as PMN-MDSCs in this study. However, it has also been noted that CD244 is useful to distinguish PMN-MDSCs from only normal neutrophils but not tumor-associated neutrophils (11). Further studies will be needed to determine the precise surface phenotypes of MDSC subsets.

The murine colon cancer cell line MC38 produced G-CSF and IL-6 at the high levels, which appeared to induce PMN-MDSCs in the peritoneal cavity and then in the systemic circulation. In this regard, the accumulation of MDSCs has been shown to depend on two distinct signaling pathways; one is associated with the expansion of immature myeloid cells and the another is associated with their pathological activation (40). In particular, G-CSF is well known as a cytokine associated with the differentiation and trafficking of granulocytic lineage and the generation of PMN-MDSCs (41), whereas IL-6 would promote the systemic accumulation of PMN-MDSCs (42). Our cytokine profile data were consistent with these previous reports. In the MC38-based PD model, G-CSF would induce the formation and trafficking of immature myeloid cells into the peritoneal cavity, and IL-6 would promote the systemic increase of MDSCs. That is, it is assumable that PMN-MDSCs would be provided from the local peritoneal cavity and spread systemically. Besides, both G-CSF and IL-6 are known to activate the signaling of signal transducer and activator of transcription 3 (STAT-3), which is strongly associated with the induction of PMN-MDSCs (43). The precise mechanisms of PMN-MDSC induction remain a significant issue that requires further investigation.

In human, recombinant human G-CSF (rhG-CSF) has become a primary therapeutic agent to prevent and recover from chemotherapy-induced myelosuppression. Some major guidelines recommend the use of rhG-CSF when there is approximately a 20% risk of febrile neutropenia (44,45). In addition, a recent meta-analysis study has shown that patients

who received chemotherapy under rhG-CSF support had better overall survival than those who did not receive rhG-CSF support (46). Therefore, the administration of rhG-CSF is reasonable as a supportive therapy for those with chemotherapy-induced myelosuppression in general. In contrast, our data of the PD model showed tumor-derived G-CSF at high levels in the peritoneal cavity and its association with poor prognosis of the tumor-bearing hosts as well as increased MDSCs. Moreover, several studies based on human gastric cancer and colon cancer have reported that high production levels of tumor-derived G-CSF correlate with tumor progression and poor prognosis (31,47). We interpreted these findings with our data that the use of rhG-CSF should be cautious when high levels of ectopic G-CSF exist particularly with PD.

Since PMN-MDSCs accounted for the large majority of $Ly6G^+$ cells and *in vivo*-compatible anti-CD244 antibody is known to exert strong effects on natural killer (NK) and T cells inadvertently (30), we alternatively used anti-Ly6G mAb to deplete PMN-MDSCs in the PD mouse model. Although the methods used in this study was not completely specific for PMN-MDSCs, our results still suggest that PMN-MDSCs contribute to PD progression. In this regard, it has been shown that the continuous use of anti-Ly6G mAb induces the reappearance of MDSCs in about a week, limiting its effectiveness by depletion-associated extramedullary granulopoiesis (48). We consider this phenomenon to be the cause of the suboptimal therapeutic efficacy of Ly6G depletion in this study. It is a subject for future verification how to target PMN-MDSCs specifically and sustainably.

PMN-MDSCs establish tumor-promoting environments and contribute to tumor progression. The mechanism of T-cell-based immunosuppression by PMN-MDSCs is proposed as follows. PMN-MDSCs exert the programmed cell death-1 (PD-1)/programmed cell death ligand-1 (PD-L1)-mediated immune checkpoint blockade (49). PMN-MDSCs also produce molecules that exert direct immunosuppression such as arginase-1 (Arg-1), nitric oxide synthase (NOS), and reactive oxygen species (ROS) (50) and promote tumor growth and metastatic spread indirectly such as vascular endothelial growth factor (VEGF), prokineticin 2 (PK2), and matrix metalloproteinase-9 (MMP-9) (51). Targeting PMN-MDSCs would solve these issues at once and thus can be a potent therapeutic target of cancer immunotherapy. In addition, our finding that the Ly6G-mediated PMN-MDSC depletion reverted the number of T cells in the peripheral blood as well as in the peritoneal cavity suggests an important perspective; the targeted therapy for PMN-MDSCs would enhance the therapeutic efficacy of T-cell-based immunotherapy. In this regard, the administration of CXCR2 inhibitor targeting PMN-MDSCs has improved the efficacy of T-cell adoptive immunotherapy (52,53). Although the conventional T-cell subsets of CD4, CD8, and Treg were not associated with PD progression in this study, those with exhaustion phenotypes, such as PD-1 or LAG3, might be associated with PD progression (54). We are currently in the process of addressing this aspect to seek for the possibility to combine PMN-MDSC-targeting therapy with immune checkpoint blockades or adoptive T-cell transfer therapies including CAR-T cell therapy (55).

Collectively, we demonstrated that PMN-MDSCs would suppress antitumor activities of T cells to induce PD progression in this study. Therefore, the targeted therapy for PMN-MDSCs may provide new therapeutic value to prevent the disease progression of PD. Furthermore, given the recent advancement of T-cell immunotherapy, our strategy may also provide a clue to develop new strategies to synergize with T-cell immunotherapy for CRC-derived PD.

Acknowledgements

Not applicable.

Funding

This work was supported by JSPS KAKENHI (grant no. 20K17650).

Availability of data and materials

The datasets used and/or analyzed during the current study are available from the corresponding author on reasonable request.

Authors' contributions

YS and KYamas mainly conceived and planned the experiments. YS, MS, KYamad, KA, AW, and EF carried out the experiments. YS, KYamas, MF, and MS contributed to the interpretation of the results. YS took the lead in writing the manuscript. KYamas, MF, MS, and YK critically revised the manuscript for intellectual content. HH, SK, TO, TM, TN, and SS provided critical feedback and helped shape the research, analysis and manuscript. All authors read and approved the manuscript and agree to be accountable for all aspects of the research in ensuring that the accuracy or integrity of any part of the work are appropriately investigated and resolved.

Ethics approval and consent to participate

The experimental procedures were approved by the Ethics Committee of Kobe University (approval no. P190404).

Patient consent for publication

Not applicable.

Competing interests

The authors declare that they have no competing interests.

References

1. Bray F, Ferlay J, Soerjomataram I, Siegel RL, Torre LA and Jemal A: Global cancer statistics 2018: GLOBOCAN estimates of incidence and mortality worldwide for 36 cancers in 185 countries. CA Cancer J Clin 68: 394-424, 2018.
2. Massalou D, Benizri E, Chevallier A, Duranton-Tanneur V, Pedeutour F, Benchimol D and Béréder JM: Peritoneal carcinomatosis of colorectal cancer: Novel clinical and molecular outcomes. Am J Surg 213: 377-387, 2017.
3. Sugarbaker PH: Colorectal cancer: Prevention and management of metastatic disease. BioMed Res Int 2014: 782890, 2014.
4. Segelman J, Granath F, Holm T, Machado M, Mahteme H and Martling A: Incidence, prevalence and risk factors for peritoneal carcinomatosis from colorectal cancer. Br J Surg 99: 699-705, 2012.

5. Klaver YL, Simkens LH, Lemmens VE, Koopman M, Teerenstra S, Bleichrodt RP, de Hingh IH and Punt CJ: Outcomes of colorectal cancer patients with peritoneal carcinomatosis treated with chemotherapy with and without targeted therapy. Eur J Surg Oncol 38: 617-623, 2012.
6. Franko J, Shi Q, Meyers JP, Maughan TS, Adams RA, Seymour MT, Saltz L, Punt CJA, Koopman M, Tournigand C, *et al*: Prognosis of patients with peritoneal metastatic colorectal cancer given systemic therapy: An analysis of individual patient data from prospective randomised trials from the analysis and research in cancers of the digestive system (ARCAD) database. Lancet Oncol 17: 1709-1719, 2016.
7. Binnewies M, Roberts EW, Kersten K, Chan V, Fearon DF, Merad M, Coussens LM, Gabrilovich DI, Ostrand-Rosenberg S, Hedrick CC, *et al*: Understanding the tumor immune microenvironment (TIME) for effective therapy. Nat Med 24: 541-550, 2018.
8. Fridman WH, Zitvogel L, Sautès-Fridman C and Kroemer G: The immune contexture in cancer prognosis and treatment. Nat Rev Clin Oncol 14: 717-734, 2017.
9. Keren L, Bosse M, Marquez D, Angoshtari R, Jain S, Varma S, Yang SR, Kurian A, Van Valen D, West R, *et al*: A Structured tumor-immune microenvironment in triple negative breast cancer revealed by multiplexed ion beam imaging. Cell 174: 1373-1387. e19, 2018.
10. Peltanova B, Raudenska M and Masarik M: Effect of tumor microenvironment on pathogenesis of the head and neck squamous cell carcinoma: A systematic review. Mol Cancer 18: 63, 2019.
11. Veglia F, Perego M and Gabrilovich D: Myeloid-derived suppressor cells coming of age. Nat Immunol 19: 108-119, 2018.
12. Gabrilovich DI, Ostrand-Rosenberg S and Bronte V: Coordinated regulation of myeloid cells by tumours. Nat Rev Immunol 12: 253-268, 2012.
13. Otsubo D, Yamashita K, Fujita M, Nishi M, Kimura Y, Hasegawa H, Suzuki S and Kakeji Y: Early-phase treatment by Low-dose 5-Fluorouracil or primary tumor resection inhibits MDSC-mediated lung metastasis formation. Anticancer Res 35: 4425-4431, 2015.
14. Tanaka T, Fujita M, Hasegawa H, Arimoto A, Nishi M, Fukuoka E, Sugita Y, Matsuda T, Sumi Y, Suzuki S, *et al*: Frequency of Myeloid-derived suppressor cells in the peripheral blood reflects the status of tumor recurrence. Anticancer Res 37: 3863-3869, 2017.
15. Youn JI, Nagaraj S, Collazo M and Gabrilovich DI: Subsets of Myeloid-Derived suppressor cells in tumor bearing mice. J Immunol 181: 5791-5802, 2008.
16. Fortin C, Huang X and Yang Y: NK cell response to vaccinia virus is regulated by myeloid-derived suppressor cells. J Immunol 189: 1843-1849, 2012.
17. Cassetta L, Baekkevold ES, Brandau S, Bujko A, Cassatella MA, Dorhoi A, Krieg C, Lin A, Loré K, Marini O, *et al*: Deciphering myeloid-derived suppressor cells: Isolation and markers in humans, mice and non-human primates. Cancer Immunol Immunother 68: 687-697, 2019.
18. Agresta L, Hoebe KHN and Janssen EM: The emerging role of CD244 signaling in immune cells of the tumor microenvironment. Front Immunol 9: 2809, 2018.
19. Wu Y, Kuang DM, Pan WD, Wan YL, Lao XM, Wang D, Li XF and Zheng L: Monocyte/macrophage-elicited natural killer cell dysfunction in hepatocellular carcinoma is mediated by CD48/2B4 interactions. Hepatology 57: 1107-1116, 2013.
20. Wherry EJ and Kurachi M: Molecular and cellular insights into T cell exhaustion. Nat Rev Immunol 15: 486-499, 2015.
21. Youn JI, Collazo M, Shalova IN, Biswas SK and Gabrilovich DI: Characterization of the nature of granulocytic myeloid-derived suppressor cells in tumor-bearing mice. J Leukoc Biol 91: 167-181, 2012.
22. Clarke P, Mann J, Simpson JF, Rickard-Dickson K and Primus FJ: Mice transgenic for human carcinoembryonic antigen as a model for immunotherapy. Cancer Res 58: 1469-1477, 1998.
23. Ojima T, Iwahashi M, Nakamura M, Matsuda K, Nakamori M, Ueda K, Naka T, Ishida K, Primus FJ and Yamaue H: Successful cancer vaccine therapy for carcinoembryonic antigen (CEA)-expressing colon cancer using genetically modified dendritic cells that express CEA and T helper-type 1 cytokines in CEA transgenic mice. Int J Cancer 120: 585-593, 2007.
24. Kilkenny C, Browne WJ, Cuthill IC, Emerson M and Altman DG: Improving bioscience research reporting: The ARRIVE guidelines for reporting animal research. PLoS Biol 8: e1000412, 2010.
25. Feldman AT and Wolfe D: Tissue processing and hematoxylin and eosin staining. Methods Mol Biol 1180: 31-43, 2014.
26. Arimoto A, Yamashita K, Hasegawa H, Sugita Y, Fukuoka E, Tanaka T, Suzuki S and Kakeji Y: Immunosuppression induced by perioperative peritonitis promotes lung metastasis. Anticancer Res 38: 4333-4338, 2018.
27. Bruger AM, Dorhoi A, Esendagli G, Barczyk-Kahlert K, van der Bruggen P, Lipoldova M, Perecko T, Santibanez J, Saraiva M, Van Ginderachter JA and Brandau S: How to measure the immunosuppressive activity of MDSC: Assays, problems and potential solutions. Cancer Immunol Immunother 68: 631-644, 2019.
28. Shang W, Tang Z, Gao Y, Qi H, Su X, Zhang Y and Yang R: LncRNA RNCR3 promotes Chop expression by sponging miR-185-5p during MDSC differentiation. Oncotarget 8: 111754-111769, 2017.
29. Schleicher U, Paduch K, Debus A, Obermeyer S, König T, Kling JC, Ribechini E, Dudziak D, Mougiakakos D, Murray PJ, *et al*: TNF-mediated restriction of arginase 1 expression in myeloid cells triggers type 2 NO synthase activity at the site of infection. Cell Rep 15: 1062-1075, 2016.
30. Agresta L, Lehn M, Lampe K, Cantrell R, Hennies C, Szabo S, Wise-Draper T, Conforti L, Hoebe K and Janssen EM: CD244 represents a new therapeutic target in head and neck squamous cell carcinoma. J Immunother Cancer 8: e000245, 2020.
31. Morris KT, Khan H, Ahmad A, Weston LL, Nofchissey RA, Pinchuk IV and Beswick EJ: G-CSF and G-CSFR are highly expressed in human gastric and colon cancers and promote carcinoma cell proliferation and migration. Br J Cancer 110: 1211-1220, 2014.
32. Kawano M, Mabuchi S, Matsumoto Y, Sasano T, Takahashi R, Kuroda H, Kozasa K, Hashimoto K, Isobe A, Sawada K, *et al*: The significance of G-CSF expression and myeloid-derived suppressor cells in the chemoresistance of uterine cervical cancer. Sci Rep 5: 18217, 2015.
33. Pilatova K, Bencsikova B, Demlova R, Valik D and Zdrazilova-Dubska L: Myeloid-derived suppressor cells (MDSCs) in patients with solid tumors: Considerations for granulocyte colony-stimulating factor treatment. Cancer Immunol Immunother 67: 1919-1929, 2018.
34. Veglia F, Sanseviero E and Gabrilovich DI: Myeloid-derived suppressor cells in the era of increasing myeloid cell diversity. Nat Rev Immunol: Feb 1, 2021 (Epub ahead of print). doi: 10.1038/s41577-020-00490-y.
35. Ceelen W, Ramsay RG, Narasimhan V, Heriot AG and De Wever O: Targeting the tumor microenvironment in colorectal peritoneal metastases. Trends Cancer 6: 236-246, 2020.
36. Toyoshima M, Tanaka Y, Matumoto M, Yamazaki M, Nagase S, Sugamura K and Yaegashi N: Generation of a syngeneic mouse model to study the intraperitoneal dissemination of ovarian cancer with in vivo luciferase imaging. Luminescence 24: 324-331, 2009.
37. Taibi A, Albouys J, Jacques J, Perrin ML, Yardin C, Durand Fontanier S and Bardet SM: Comparison of implantation sites for the development of peritoneal metastasis in a colorectal cancer mouse model using non-invasive bioluminescence imaging. PLoS One 14: e0220360, 2019.
38. Lee YS, Lee WS, Kim CW, Lee SJ, Yang H, Kong SJ, Ning J, Yang KM, Kang B, Kim WR, *et al*: Oncolytic vaccinia virus reinvigorates peritoneal immunity and cooperates with immune checkpoint inhibitor to suppress peritoneal carcinomatosis in colon cancer. J Immunother Cancer 8: e000857, 2020.
39. Cassim S and Pouyssegur J: Tumor microenvironment: A metabolic player that shapes the immune response. Int J Mol Sci 21: 157, 2019.
40. Condamine T and Gabrilovich DI: Molecular mechanisms regulating myeloid-derived suppressor cell differentiation and function. Trends Immunol 32: 19-25, 2011.
41. Waight JD, Hu Q, Miller A, Liu S and Abrams SI: Tumor-Derived G-CSF facilitates neoplastic growth through a granulocytic myeloid-derived suppressor cell-dependent mechanism. PLoS One 6: e27690, 2011.
42. Weber R, Groth C, Lasser S, Arkhypov I, Petrova V, Altevogt P, Utikal J and Umansky V: IL-6 as a major regulator of MDSC activity and possible target for cancer immunotherapy. Cell Immunol 359: 104254, 2021.
43. Kramer ED and Abrams SI: Granulocytic myeloid-derived suppressor cells as negative regulators of anticancer immunity. Front Immunol 11: 1963, 2020.
44. Aapro MS, Cameron DA, Pettengell R, Bohlius J, Crawford J, Ellis M, Kearney N, Lyman GH, Tjan-Heijnen VC, Walewski J, *et al*: EORTC guidelines for the use of granulocyte-colony stimulating factor to reduce the incidence of chemotherapy-induced febrile neutropenia in adult patients with lymphomas and solid tumours. Eur J Cancer 42: 2433-2453, 2006.

45. Becker PS, Griffiths EA, Alwan LM, Bachiashvili K, Brown A, Cool R, Curtin P, Dinner S, Gojo I, Hicks A, *et al*: NCCN guidelines insights: Hematopoietic growth factors, version 1.2020. J Natl Compr Canc Netw 18: 12-22, 2020.
46. Lyman GH, Yau L, Nakov R and Krendyukov A: Overall survival and risk of second malignancies with cancer chemotherapy and G-CSF support. Ann Oncol 29: 1903-1910, 2018.
47. Fan Z, Li Y, Zhao Q, Fan L, Tan B, Zuo J, Hua K and Ji Q: Highly expressed granulocyte colony-stimulating factor (G-CSF) and granulocyte colony-stimulating factor receptor (G-CSFR) in human gastric cancer leads to poor survival. Med Sci Monit 24: 1701-1711, 2018.
48. Moses K, Klein JC, Männ L, Klingberg A, Gunzer M and Brandau S: Survival of residual neutrophils and accelerated myelopoiesis limit the efficacy of antibody-mediated depletion of Ly-6G$^+$ cells in tumor-bearing mice. J Leukoc Biol 99: 811-823, 2016.
49. Law AM, Valdes-Mora F and Gallego-Ortega D: Myeloid-derived suppressor cells as a therapeutic target for cancer. Cells 9: 561, 2020.
50. Vetsika EK, Koukos A and Kotsakis A: Myeloid-Derived suppressor cells: Major figures that shape the immunosuppressive and angiogenic network in cancer. Cells 8: 1647, 2019.
51. Coffelt SB, Wellenstein MD and de Visser KE: Neutrophils in cancer: Neutral no more. Nature Reviews Cancer 16: 431-446, 2016.
52. Steele CW, Karim SA, Leach JDG, Bailey P, Upstill-Goddard R, Rishi L, Foth M, Bryson S, McDaid K, Wilson Z, *et al*: CXCR2 inhibition profoundly suppresses metastases and augments immunotherapy in pancreatic ductal adenocarcinoma. Cancer Cell 29: 832-845, 2016.
53. Sun L, Clavijo PE, Robbins Y, Patel P, Friedman J, Greene S, Das R, Silvin C, Van Waes C, Horn LA, *et al*: Inhibiting myeloid-derived suppressor cell trafficking enhances T cell immunotherapy. JCI Insight 4: e126853, 2019.
54. Kurachi M: CD8$^+$ T cell exhaustion. Semin Immunopathol 41: 327-337, 2019.
55. Martinez M and Moon EK: CAR T cells for solid tumors: New strategies for finding, infiltrating, and surviving in the tumor microenvironment. Front Immunol 10: 128, 2019.